

# Nucleon to $\Delta$ and $\Delta$ form factors in Lattice QCD

Constantia Alexandrou

*Department of Physics, University of Cyprus, P.O. Box 20537, 1678 Nicosia, Cyprus and  
Computation-based Science and Technology Research Center, The Cyprus Institute, P.O. Box  
27456, 1645 Nicosia, Cyprus*

**Abstract.** We present recent lattice QCD results on the electroweak nucleon to  $\Delta$  transition and  $\Delta$  form factors using dynamical fermion gauge configurations with a lowest pion mass of about 300 MeV, with special emphasis in the determination of the sub-dominant quadrupole  $N\gamma^* \rightarrow \Delta$  and  $\Delta$  electromagnetic form factors.

**Keywords:** Transition form factors, Lattice QCD

**PACS:** 11.15.Ha, 12.38.Gc, 13.40.Gp, 14.20.Gk

## INTRODUCTION

There is a number of recent lattice QCD calculations of the electroweak form factors of the nucleon [1]. The main focus of this presentation is the evaluation of the electroweak nucleon (N) to  $\Delta$  and  $\Delta$  form factors (FFs). In  $N\gamma^* \rightarrow \Delta$  the dominant magnetic dipole FF,  $G_{M1}^*$ , is precisely measured and it therefore serves, like in the case of the electromagnetic (EM) FFs of the nucleon, as a benchmark of the lattice QCD methodology. The sub-dominant quadrupole FFs  $G_{E2}^*$  and  $G_{C2}^*$  have also been studied extensively, since their value carries information on the deformation in the N/ $\Delta$  system. In order to calculate them in lattice QCD, one applies several improvements to attain good enough accuracy. The dominant axial N to  $\Delta$  form factors  $C_5^A$  and  $C_6^A$  can also be calculated within lattice QCD. They correspond to the nucleon axial,  $G_A$ , and nucleon induced pseudo-scalar,  $G_p$ , FFs and provide important input for phenomenological models and chiral effective theories. Furthermore, the evaluation of the  $\pi N\Delta$  coupling enables us to check the validity of PCAC and the associated non-diagonal Goldberger-Treiman relation.

The FFs of the  $\Delta$  are difficult to measure experimentally due to the  $\Delta$  short lifetime. Only the magnetic moment of the  $\Delta$  is measured albeit with large uncertainty. Thus lattice QCD can provide a valuable input on the  $\Delta$  FFs enabling for instance the determination of the  $\Delta$  charge distribution in the infinite momentum frame [2]. Due to the 3/2-spin structure of the  $\Delta$ , there are two Goldberger-Treiman relations, which can be examined by calculating, besides the axial  $\Delta$  FFs the pseudo-scalar ones. Having the EM and axial FFs for the N/ $\Delta$  system enables a combined chiral fit to determine the coupling constants that enter in chiral effective models.

Recently there has been a lot of progress in the calculation of hadron masses and nucleon structure using dynamical lattice QCD simulations [3]. The computational cost of these simulations can be parameterized as a function of the lattice spacing  $a$ , the lattice spatial extent  $L$  and the pion mass,  $m_\pi$ , as  $C_{\text{sim}} \propto \left(\frac{300\text{MeV}}{m_\pi}\right)^{c_m} \left(\frac{L}{2\text{fm}}\right)^{c_L} \left(\frac{0.1\text{fm}}{a}\right)^{c_a}$ . The coefficients  $c_m$ ,  $c_L$  and  $c_a$  depend on the type of discretized action. Based on current

simulations the cost at the physical point is estimated of  $\mathcal{O}(1)$  Teraflop-year.

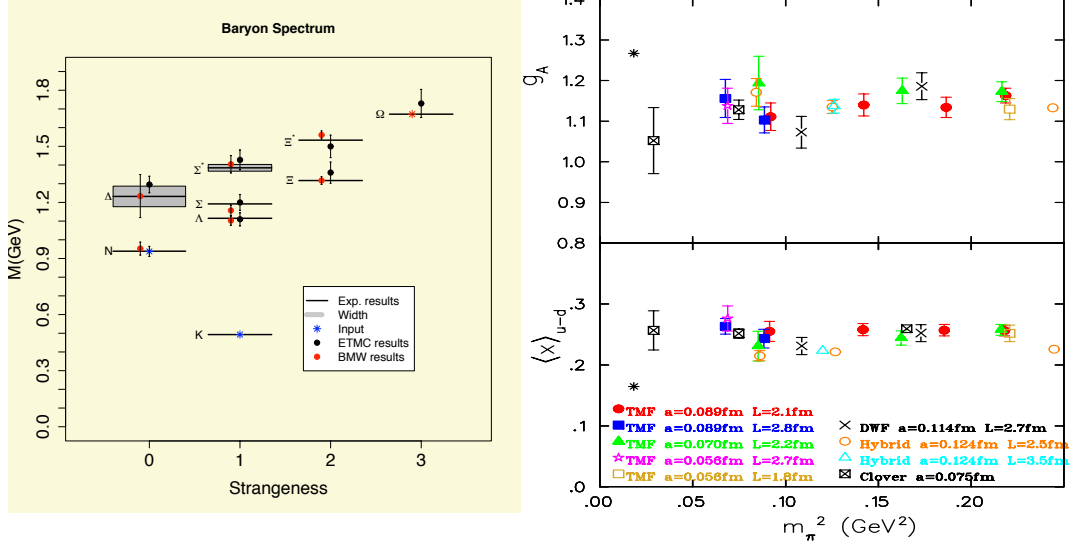


**FIGURE 1.** Left: The low-lying baryon spectrum computed using  $N_f = 2 + 1$  Clover [4] and  $N_f = 2$  twisted mass fermions (TMF) [5]; Upper right: The nucleon axial charge [6]; Lower right: The nucleon isovector moment of the unpolarized quark distribution [7]. The physical point is shown by the asterisk.

In Fig. 1 we show recent results on the low-lying baryon spectrum obtained by the BMW Collaboration using  $N_F = 2 + 1$  Clover fermions and the ETM Collaboration using  $N_F = 2$  twisted mass fermions. Both collaborations used 3 lattice spacings to extrapolate the results to the continuum limit. One observes that the results using different discretization schemes are in agreement and that both reproduce the experimental values. This is a significant validation of lattice QCD techniques.

The electric  $G_E(q^2)$  and magnetic  $G_M(q^2)$  Sachs form factors (FFs) as well as the axial-vector FFs  $G_A(q^2)$  and  $\bar{G}_p(q^2)$  of the nucleon have also been studied by several lattice groups using dynamical simulations down to lowest pion mass of typically  $\sim 250$  MeV. Lattice data are in general agreement, but still show discrepancies with experiment. In Fig. 1 we compare recent results from various collaborations on the nucleon axial charge and isovector moment of the unpolarized quark distribution. Whereas there is an overall agreement among lattice results the experimental values are not reproduced (see Ref. [1] for more details).

## $N\gamma^* \rightarrow \Delta$ TRANSITION FORM FACTORS

The  $N\gamma^* \rightarrow \Delta$  transition is written in terms of three Sachs FFs:

$$\langle \Delta(p', s') | j_\mu | N(p, s) \rangle = \mathcal{A} \bar{u}_\sigma(p', s') \left[ G_{M1}^*(q^2) K_{\sigma\mu}^{M1} + G_{E2}^*(q^2) K_{\sigma\mu}^{E2} + G_{C2}^* K_{\sigma\mu}^{C2} \right] u(p, s) \quad (1)$$

with  $\mathcal{A} = i\sqrt{\frac{2}{3}} \left( \frac{m_{\Delta N}}{E_\Delta(\mathbf{p}') E_N(\mathbf{p})} \right)^{1/2}$ . There is a wealth of experimental information on the  $N\gamma^* \rightarrow \Delta$  transition [8]: The dominant magnetic dipole FF,  $G_{M1}^*$ , is well mea-

sured and the electric  $G_{E2}^*$  and Coulomb  $G_{C2}^*$  FFs are found to be non-zero signaling a deformation in the nucleon/ $\Delta$ -system. The deformation is probed via the ratios:  $R_{EM}(\text{EMR}) = -\frac{G_{E2}^*(Q^2)}{G_{M1}^*(Q^2)}$ , and  $R_{SM}(\text{CMR}) = -\frac{|\vec{q}|}{2m_\Delta} \frac{G_{C2}^*(Q^2)}{G_{M1}^*(Q^2)}$ , in the rest frame of the  $\Delta$ . As shown in Fig. 2, precise data strongly “suggest” deformation of the N and/or  $\Delta$  [9, 10]. New data on CMR at low momentum transfer are currently being analyzed [11].

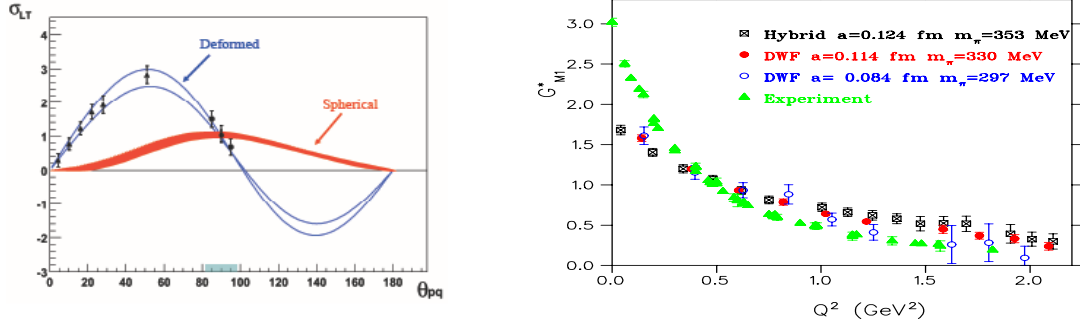
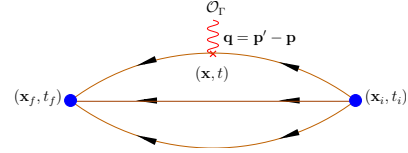


**FIGURE 2.** Left: The  $\sigma_{LT}$  of the  $p(e, e'p)\pi^0$  reaction at  $Q^2 = 0.127 \text{ GeV}^2$  [9]; Right: Experimental and lattice QCD results on the magnetic dipole FF  $G_{M1}^*$  as a function of  $Q^2 = -(p' - p)^2$ .

The lattice evaluation involves the computation of two-point and three-point functions:

$$G(\vec{q}, t) = \sum_{\vec{x}_f} e^{-i\vec{x}_f \cdot \vec{q}} \Gamma^4 \langle J_h(\vec{x}_f, t_f) \bar{J}_h(0) \rangle$$

$$G^{\mu\nu}(\Gamma, \vec{q}, t) = \sum_{\vec{x}_f, \vec{x}} e^{i\vec{x} \cdot \vec{q}} \Gamma \langle J_h(\vec{x}_f, t_f) \mathcal{O}^\mu(\vec{x}, t) \bar{J}_h(0) \rangle$$



where  $\bar{J}_h(x, t)$  is an interpolating field creating a state with the quantum numbers of the baryon  $h$  and we have taken  $t_i = 0$ . One computes the three-point function at various  $t$ -values of the current insertion  $\mathcal{O}_\Gamma$ , which, for large  $t_f$  and  $t$  and taking an appropriate ratio with two-point functions, yields the matrix element of Eq. (1).

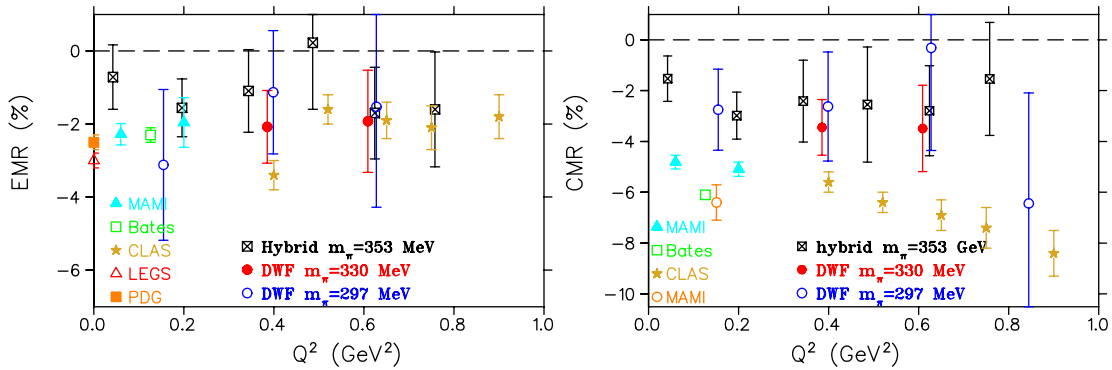


**FIGURE 3.** Results on EMR (left) and CMR (right).

In order to extract the sub-dominant quadrupole FFs one constructs optimized sources to isolate them from the dominant dipole and uses the coherent sink technique to increase statistics. Recent lattice results are shown in Figs. 2 and 3 using a hybrid action of dynamical staggered sea and domain wall valence quarks, as well as  $N_F = 2 + 1$

dynamical domain wall fermions (DWF), simulated by the RBC-UKQCD with lowest pion mass of about 300 MeV [12]. The slope of  $G_{M1}^*$  at low  $Q^2$  remains smaller than what is observed in experiment underestimating  $G_{M1}^*(0)$  i.e. one observes the same effect as for the nucleon form factors. Since  $G_{E2}^*$  and  $G_{C2}^*$  are underestimated at low  $Q^2$  like  $G_{M1}^*$  taking ratios may remove some of these discrepancies. Indeed the EMR shown in Fig. 3 is in better agreement with experiment, whereas CMR approaches the experimental values as the pion mass is lowered. Despite the increased statistics the errors on the sub-dominant ratios are large and to reduce the errors as  $m_\pi$  approaches its physical value one would need to increase significantly the number of statistically independent evaluations.

## N - $\Delta$ AXIAL-VECTOR AND PSEUDO-SCALAR FORM FACTORS

The N -  $\Delta$  axial-vector matrix element  $\langle \Delta(p', s') | A_\mu^3 | N(p, s) \rangle$  is written as

$$\not{A} \bar{u}^\lambda(p', s') \left[ \left( \frac{C_3^A(q^2)}{m_N} \gamma^\nu + \frac{C_4^A(q^2)}{m_N^2} p'^\nu \right) (g_{\lambda\mu} g_{\rho\nu} - g_{\lambda\rho} g_{\mu\nu}) q^\rho + C_5^A(q^2) g_{\lambda\mu} + \frac{C_6^A(q^2)}{m_N^2} q_\lambda q_\mu \right] u(p, s), \quad (2)$$

whereas the N -  $\Delta$  matrix element of the pseudo-scalar current is given by

$$2m_q \langle \Delta(p', s') | P^3 | N(p, s) \rangle = \not{A} \frac{f_\pi m_\pi^2 G_{\pi N \Delta}(q^2)}{m_\pi^2 - q^2} \bar{u}_\nu(p', s') \frac{q_\nu}{2m_N} u(p, s) \quad (3)$$

Using the axial Ward identity and pion pole dominance one obtains the non-diagonal Goldberger-Treiman (GT) relation,  $G_{\pi N \Delta}(q^2) f_\pi = 2m_N C_5^A(q^2)$ . In Fig. 4 we show results on the dominant axial FF  $C_5^A$  and on the ratio  $G_{\pi N \Delta}(Q^2) f_\pi / 2m_N C_5^A(Q^2)$ , which should be unity if the GT relation holds. This ratio approaches unity for  $Q^2 > 0.5 \text{ GeV}^2$  [12].

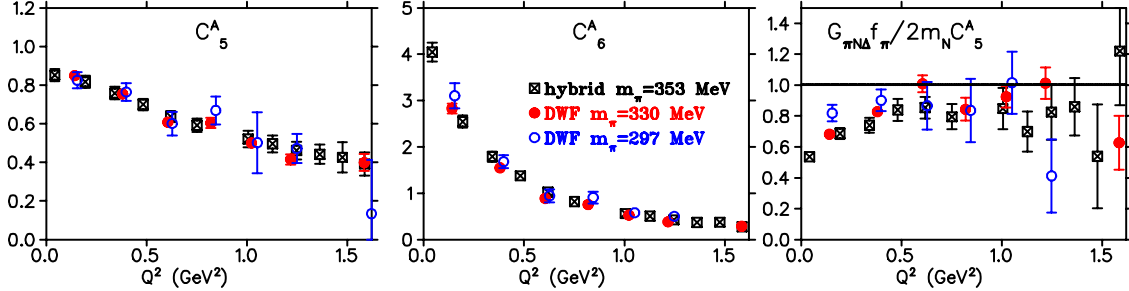


FIGURE 4. The dominant axial and pseudo-scalar N to  $\Delta$  FFs using a hybrid action and DWF.

## $\Delta$ FORM FACTORS

The  $\Delta$  matrix element of the electromagnetic current  $\langle \Delta(p', s') | j^\mu | \Delta(p, s) \rangle$  is given by

$$-\bar{u}_\alpha(p', s') \left\{ \left[ F_1^*(q^2) g^{\alpha\beta} + F_3^*(q^2) \frac{q^\alpha q^\beta}{(2M_\Delta)^2} \right] \gamma^\mu + \left[ F_2^*(q^2) g^{\alpha\beta} + F_4^*(q^2) \frac{q^\alpha q^\beta}{(2M_\Delta)^2} \right] \frac{i\sigma^{\mu\nu} q_\nu}{2M_\Delta} \right\} u_\beta(p, s) \quad (4)$$

with e.g. the quadrupole FF given by:  $G_{E2} = (F_1^* - \tau F_2^*) - \frac{1}{2}(1 + \tau)(F_3^* - \tau F_4^*)$ , where  $\tau \equiv -q^2/(4M_\Delta^2)$ . Using lattice results on  $G_{E2}$  one can obtain the transverse charge density of a  $\Delta$  in the infinite momentum frame [13, 14]. This is shown in Fig. 5, where a  $\Delta$  with spin 3/2 projection along the x-axis is elongated along the spin axis [13]. In the same figure we also show the corresponding charge density of the  $\Omega^-$ , which shows a similar deformation as the  $\Delta$  [15].

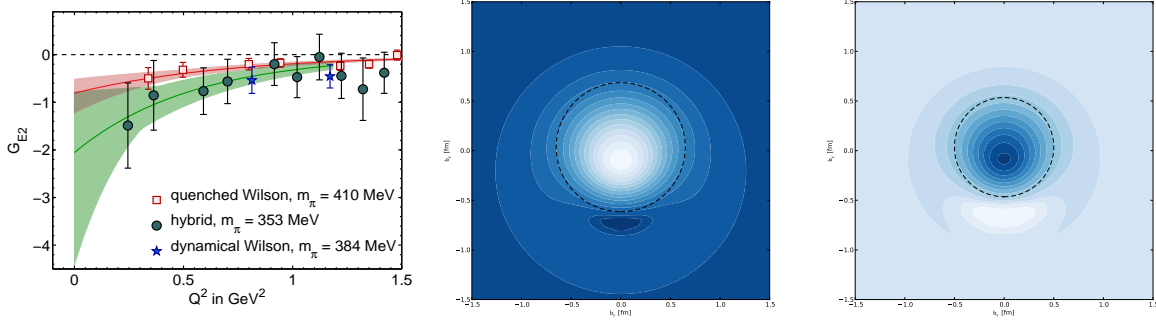


**FIGURE 5.** Left: Lattice results on the  $\Delta$  electric quadrupole FF; Contours of  $\Delta$  (middle) and  $\Omega^-$  (right) [15], with 3/2 spin projection along the x-axis. Dark colors denote small values.

The  $\Delta$  matrix elements of the axial-vector current  $\langle \Delta(p', s') | A_\mu^3 | \Delta(p, s) \rangle$  is given by

$$\frac{-1}{2} \bar{u}_\alpha(p', s') \left[ g^{\alpha\beta} \left( g_1(q^2) \gamma^\mu \gamma^5 + g_3(q^2) \frac{q^\mu}{2M_\Delta} \gamma^5 \right) + \frac{q^\alpha q^\beta}{4M_\Delta^2} \left( h_1(q^2) \gamma^\mu \gamma^5 + h_3(q^2) \frac{q^\mu}{2M_\Delta} \gamma^5 \right) \right] u_\beta(p, s) \quad (5)$$

and of the pseudo-scalar current  $\langle \Delta(p', s') | P^3 | \Delta(p, s) \rangle$  by

$$-\bar{u}_\alpha(p', s') \frac{f_\pi m_\pi^2}{2m_q(m_\pi^2 - q^2)} \left[ g^{\alpha\beta} G_{\pi\Delta\Delta}(q^2) \gamma^5 + \frac{q^\alpha q^\beta}{4M_\Delta^2} H_{\pi\Delta\Delta}(q^2) \gamma^5 \right] u_\beta(p, s). \quad (6)$$

The  $\Delta$  axial charge is derived from  $g_1(0)$  [16, 17], whereas there are two  $\pi\Delta\Delta$  pseudo-scalar FFs.

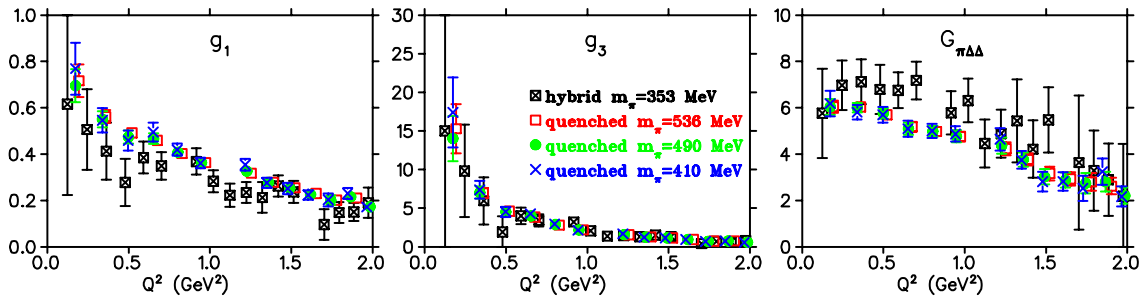


**FIGURE 6.** Lattice QCD results on the dominant axial and pseudo-scalar  $\Delta$  FFs in the quenched theory and using a hybrid action [17].

$G_{\pi\Delta\Delta}(0)$  is non-zero and can be identified as the  $\pi - \Delta$  coupling. Lattice QCD results on the dominant axial  $\Delta$  FFs  $g_1$  and  $g_3$  as well as on  $G_{\pi\Delta\Delta}$  are shown in Fig. 6. One can derive two Goldberger-Treiman relations:  $f_\pi G_{\pi\Delta\Delta}(q^2) = m_\Delta g_1(q^2)$ , and  $f_\pi H_{\pi\Delta\Delta}(q^2) = m_\Delta h_1(q^2)$ , which can be tested using lattice QCD results.

## CONCLUSIONS

We have shown that lattice QCD successfully reproduces the low-lying baryon spectrum using different discretization schemes. There is an on-going investigation of nucleon structure by a number of lattice collaborations. Similar techniques can be applied to study transitions and resonant properties and we have applied these methods in the study of the  $N$  to  $\Delta$  electroweak transition FFs as well as the  $\Delta$  FFs. The latter are difficult to measure experimentally and therefore lattice QCD provides valuable input on these quantities. Having lattice QCD results on the  $N$ - $\Delta$  system one can use, for the first time, chiral perturbation theory to extract the axial couplings  $g_A$ ,  $c_A$  and  $g_\Delta$  from a combined chiral fit to the lattice results on the nucleon and  $\Delta$  axial charges and the axial  $N$  to  $\Delta$  form factor  $C_5(0)$  [17]. Applying such a fit to lattice results in the pion mass range from 500 MeV to 300 MeV, still does not reproduce the experimental value of  $g_A$ . Current lattice QCD simulations reaching pion masses below 200 MeV are now becoming available and these simulations, combined with a detailed study of lattice systematics [18], are expected to shed light on the origins of the observed discrepancies.

## ACKNOWLEDGMENTS

I would like to thank my collaborators T. Korzec, G. Koutsou, E. Gregory, J. W. Negele, T. Sato, A. Tsapalis and M. Vanderhaeghen whose contributions made this work possible. I am grateful to G. Koutsou and A. Tsapalis for providing comments to the manuscript. This research was partly supported by the Cyprus Research Promotion Foundation (R.P.F) under grant  $\Delta$  IEΘNHΣ/ΣΤΟΧΟΣ/0308/07 and by the Research Executive Agency of the European Union under Grant Agreement number PITN-GA-2009-238353 (ITN STRONGnet). Domain wall fermion configurations were provided by the RBC-UKQCD collaborations and the forward propagators by the LHPC and the use of Chroma software [19].

## REFERENCES

1. C. Alexandrou, *PoS LATTICE2010*, 001 (2010), 1011.3660.
2. C. Alexandrou, et al., *PoS CD09*, 092 (2009), 0910.3315.
3. K. Jansen, *PoS LATTICE2008*, 010 (2008), 0810.5634.
4. S. Durr, et al., *Science* **322**, 1224–1227 (2008).
5. C. Alexandrou, et al., *Phys.Rev.* **D80**, 114503 (2009), 0910.2419.
6. C. Alexandrou, et al., *Phys.Rev.* **D83**, 045010 (2011), 1012.0857.
7. C. Alexandrou, et al., *Phys.Rev.* **D83**, 114513 (2011), 1104.1600.
8. A. M. Bernstein, and C. N. Papanicolas, *AIP Conf. Proc.* **904**, 1–22 (2007), 0708.0008.
9. C. N. Papanicolas, *Eur. Phys. J.* **A18**, 141 (2003).
10. N. F. Sparveris, et al., *Phys. Rev. Lett.* **94**, 022003 (2005), nucl-ex/0408003.
11. N. F. Sparveris, private communication (2011), hall A, JLab.
12. C. Alexandrou, G. Koutsou, J. Negele, Y. Proestos, and A. Tsapalis, *Phys.Rev.* **D83**, 014501 (2011).
13. C. Alexandrou, et al., *Nucl. Phys.* **A825**, 115–144 (2009), 0901.3457.
14. C. Alexandrou, et al., *Phys. Rev.* **D79**, 014507 (2009), 0810.3976.
15. C. Alexandrou, T. Korzec, G. Koutsou, J. W. Negele, and Y. Proestos, *Phys. Rev.* **D82**, 034504 (2010).
16. C. Alexandrou, et al., *PoS LATTICE2010*, 141 (2010), 1011.0411.
17. C. Alexandrou, et al. (2011), 1106.6000.
18. S. Dinter, C. Alexandrou, M. Constantinou, V. Drach, K. Jansen, et al. (2011), 1108.1076.
19. R. G. Edwards, and B. Joo, *Nucl. Phys. Proc. Suppl.* **140**, 832 (2005), hep-lat/0409003.